

A self-powered and sensitive terahertz photodetection based on $PdSe_2$

Jie Zhou(周洁), Xueyan Wang(王雪妍), Zhiqingzi Chen(陈支庆子), Libo Zhang(张力波), Chenyu Yao(姚晨禹), Weijie Du(杜伟杰), Jiazhen Zhang(张家振), Huaizhong Xing(邢怀中), Nanxin Fu(付南新), Gang Chen(陈刚), and Lin Wang(王林)

Citation: Chin. Phys. B, 2022, 31 (**5**): 050701. DOI: 10.1088/1674-1056/ac4908
Journal homepage: http://cpb.iphy.ac.cn; http://iopscience.iop.org/cpb

What follows is a list of articles you may be interested in

Design of cylindrical conformal transmitted metasurface for orbital angular momentum vortex wave generation

Ben Fu(付犇), Shi-Xing Yu(余世星), Na Kou(寇娜), Zhao Ding(丁召), and Zheng-Ping Zhang(张正平)
Chin. Phys. B, 2022, 31 (**4**): 040703. DOI: 10.1088/1674-1056/ac3a65

A terahertz on-chip InP-based power combiner designed using coupled-grounded coplanar waveguide lines

Huali Zhu(朱华利), Yong Zhang(张勇), Kun Qu(屈坤), Haomiao Wei(魏浩淼), Yukun Li(黎雨坤), Yuehang Xu(徐跃杭), and Ruimin Xu(徐锐敏)
Chin. Phys. B, 2021, 30 (**12**): 120701. DOI: 10.1088/1674-1056/ac05af

Investigation of copper sulfate pentahydrate dehydration by terahertz time-domain spectroscopy

Yuan-Yuan Ma(马媛媛), Hao-Chong Huang(黄昊翀), Si-Bo Hao(郝思博), Wei-Chong Tang(汤伟冲), Zhi-Yuan Zheng(郑志远), Zi-Li Zhang(张自力)
Chin. Phys. B, 2019, 28 (**6**): 060702. DOI: 10.1088/1674-1056/28/6/060702

Theoretical models for designing a 220-GHz folded waveguide backward wave oscillator

Cai Jin-Chi, Hu Lin-Lin, Ma Guo-Wu, Chen Hong-Bin, Jin Xiao, Chen Huai-Bi
Chin. Phys. B, 2015, 24 (**6**): 060701. DOI: 10.1088/1674-1056/24/6/060701

Infrared transparent frequency selective surface based on iterative metallic meshes

Yu Miao, Xu Nian-Xi, Gao Jin-Song
Chin. Phys. B, 2015, 24 (**3**): 030701. DOI: 10.1088/1674-1056/24/3/030701

A self-powered and sensitive terahertz photodetection based on $PdSe_2$

Jie Zhou(周洁)[1,2], Xueyan Wang(王雪妍)[1,2], Zhiqingzi Chen(陈支庆子)[2], Libo Zhang(张力波)[2], Chenyu Yao(姚晨禹)[2], Weijie Du(杜伟杰)[1], Jiazhen Zhang(张家振)[2], Huaizhong Xing(邢怀中)[2], Nanxin Fu(付南新)[2], Gang Chen(陈刚)[2], and Lin Wang(王林)[1,2,†]

[1] *Mathematics and Science College, Shanghai Normal University, Shanghai* 200233, *China*
[2] *Shanghai Institute of Technical Physics, State Key Laboratory of Infrared Physics, Chinese Academy of Sciences, Shanghai* 200083, *China*

(Received 2 November 2021; revised manuscript received 17 December 2021; accepted manuscript online 7 January 2022)

With the rapid development of terahertz technology, terahertz detectors are expected to play a key role in diverse areas such as homeland security and imaging, materials diagnostics, biology, medical sciences, and communication. Whereas self-powered, rapid response, and room temperature terahertz photodetectors are confronted with huge challenges. Here, we report a novel rapid response and self-powered terahertz photothermoelectronic (PTE) photodetector based on a low-dimensional material: palladium selenide ($PdSe_2$). An order of magnitude performance enhancement was observed in photodetection based on $PdSe_2$/graphene heterojunction that resulted from the integration of graphene and enhanced the Seebeck effect. Under 0.1-THz and 0.3-THz irradiations, the device displays a stable and repeatable photoresponse at room temperature without bias. Furthermore, rapid rise (5.0 μs) and decay (5.4 μs) times are recorded under 0.1-THz irradiation. Our results demonstrate the promising prospect of the detector based on $PdSe_2$ in terms of air-stable, suitable sensitivity and speed, which may have great application in terahertz detection.

Keywords: two-dimensional material, terahertz photodetector, photothermoelectric (PTE) effect

PACS: 07.57.Hm, 73.40.–c, 85.60.Gz **DOI:** 10.1088/1674-1056/ac4908

1. Introduction

Due to the excellent application potential of terahertz in security, medical imaging, material identification, communications, and astronomical detection, photodetectors that can work in the terahertz band have attracted a lot of research interest.[1–4] In particular, the demanding for self-powered, rapid response, and room temperature terahertz photodetectors is becoming more urgent within terahertz field that requiring portable, cost-effective system. However, commercially available detectors are difficult to meet these requirements. Among them, terahertz thermal detectors (such as Golay and bolometers) have a slow response speed, prohibitive cost of material, complex manufacturing techniques, and require cryogenic cooling to obtain excellent noise equivalent power (NEP) for the most part.[5,6]

The photodetectors based on the photothermoelectronic (PTE) effect have unique advantages of self-powered capability, low power consumption, and room temperature operation. From the perspective of practical applications, these advantages enable the terahertz detector based on the PTE effect to meet the requirements of energy-saving room temperature operation.[7,8] In the meantime, a vast range of novel low-dimensional materials such as graphene, black phosphorus (BP) and molybdenum disulfide (MoS_2), have been considered as potential PTE materials for terahertz photo detection. Recently, an emerging high-mobility two-dimensional (2D) transition-metal dichalcogenides (TMDs), palladium selenide ($PdSe_2$), has been predicted to have high mobility of up to 4.0×10^4 $cm^2 \cdot V^{-1} \cdot s^{-1}$ and good air stability.[9] Importantly, $PdSe_2$ has been confirmed to be a thermoelectric material. The thermoelectric figure of merit (ZT) value of $PdSe_2$ can reach up to 1.2, which is much larger than the common thermoelectric material: Bi_2Te_3 and some other TMDs.[10] Lan *et al.* found weak anisotropic characters for the p-type and n-type Seebeck coefficients through first-principles calculations. In contrast, the Seebeck coefficient and the y-direction performance were superior to it along the atomic plane.[11] What is more, the Seebeck coefficient of $PdSe_2$ will change with doping concentration. In the low-doping concentrations, the Seebeck coefficient of $PdSe_2$ can reach 600 $\mu V \cdot K^{-1}$ at room temperature. The high Seebeck coefficient of low-dimensional material: palladium selenide ($PdSe_2$) can be beneficial to PTE photodetectors.[12] Contrary to the traditional heterostructure derived from epitaxial growth, the interface in the low-dimension vdW heterostructure is less restricted by the "lattice mismatching", which is important to devise novel functionality.[13]

The excellent performance of the few layers of $PdSe_2$ has attracted the attention of many scholars. Liang *et al.* demonstrate a high-performance broadband $PdSe_2$ photodetector for visible and infrared light.[14] A highly polarization-sensitive, broadband, and self-powered photodetector based on graphene/$PdSe_2$/germanium heterojunction was also reported, with a response speed as fast as nanoseconds, subsequently.[15] In addition, the heterostructure photodetector based on a new family of 2D nanosheets: TMDs,

[†]Corresponding author. E-mail: wanglin@mail.sitp.ac.cn

© 2022 Chinese Physical Society and IOP Publishing Ltd

the $PdSe_2/WS_2$ device exhibited a broad detection range from visible light to infrared and rapid response speed (∼ 100 ms).[16,17] Recently, a new vdW field-effect transistor (FET) composed of $MoTe_2$ and $PdSe_2$ was reported, which showed a high rectification ratio and rapid response speed.[18] So far, $PdSe_2$ has achieved photodetection in the visible and infrared bands, but its application in the terahertz band still lied over the horizon.

In this work, we report the design of a PTE photodetector based on the $PdSe_2$ flake that demonstrates the photodetection capability from microwave to terahertz band. The paper organizes as follows: first, the preparation process of the device is introduced in detail; then we show the morphology and photoelectric performance characterization results of our devices. Responsivity (R) of the devices based on $PdSe_2$ can achieve up to 13 $mV{\cdot}W^{-1}$ in the microwave frequency band. And, the device is exploited by introducing vdW heterostructure, rapid response speed (4 μs) and high responsivity (54.2 $V{\cdot}W^{-1}$) at 0.3 THz is achieved without bias.

2. Research method

The $PdSe_2$ and graphene flakes are obtained via the scotch tape method, followed by the optical-microscopy for picking up high-quality flakes. After achieving good interface coupling, the metal electrodes were defined by electron beam lithography, thermal evaporation, and lift-off process. The device's surface morphology was examined by using atomic force microscopy (AFM). Broadband response test system, including visible light, infrared, microwave, terahertz wave, is composed of laser source from visible band to infrared band, a microwave source (Agilent E8257D) with electrical modulation, a preamplifier, a lock-in amplifier, a Keithley 4200 semiconductor parameter analyzer and a high-speed sampling oscilloscope. We used this system to characterize the photoelectric performance of the device under different irradiation, and the signal is acquired through the preamplifier.

3. Results and discussion

As could be seen from Figs. 1(a) and 1(b), each layer of the $PdSe_2$ lattice consists of three atomic planes. The Pd atom is located in the middle plane and covalently bonded with four Se atoms from the top and bottom layers to form a corrugated structure. The pentagon structure cannot cover the entire plane naturally, but the unique wrinkled structure of $PdSe_2$ gives it a chance to exist, and it also has fairly good air stability. A three-dimensional (3D) schematic diagram of the photodetector based on $PdSe_2$ with a typical field-effect transistor (FET) configuration is shown in Fig. 1(c). Source and drain electrodes are contacted $PdSe_2$ flake, which is located on a silicon wafer of high resistance. The illustration is an optical image of a simple photodetector based on $PdSe_2$. Figure 1(d) is the switch photoelectric characterization of the detector in the inset, where photocurrent under 0.04-THz illumination is about 5 nA. Raman spectrum and atomic force microscope (AFM) are used to characterize the channel, as shown in the illustration of Fig. 1(c). The surface topography of the device was confirmed by AFM, with the results shown in Fig. 1(e), from which a uniformity in thickness can be observed. And the multilayer structure composed of Cr/Au (∼ 70 nm) and $PdSe_2$ (∼ 100 nm) can also be distinguished clearly. The Raman spectrum in Fig. 1(f) shows four prominent peaks at 144 cm^{-1}, 207 cm^{-1}, 223 cm^{-1}, and 257 cm^{-1} due to $A_g{}^1B_{1g}{}^1$, $A_g{}^1$, $B_{1g}{}^1$, and $A_g{}^3$ phonon peaks, respectively.[19]

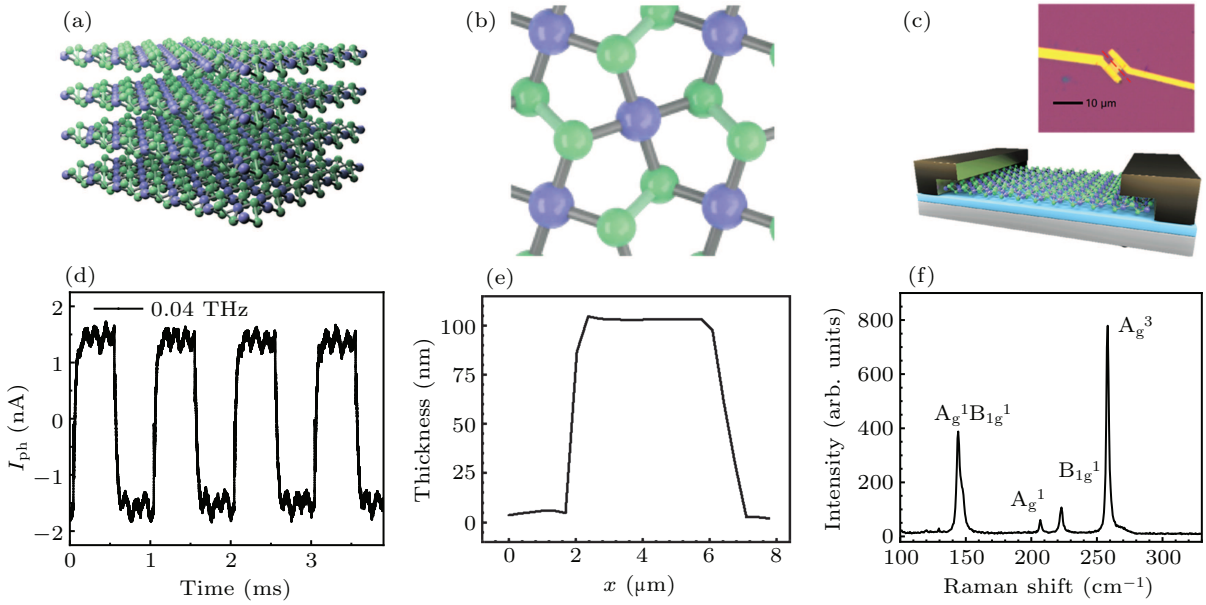


Fig. 1. Basic characterization of 2D $PdSe_2$: (a) crystallographic structure of fewer layer pentagonal $PdSe_2$. The blue spheres represent Pd atoms and green spheres are for Se atoms. (b) Puckered crystal structure of monolayer $PdSe_2$ in top view. (c) The schematic and optical images of the photodetector based on $PdSe_2$. (d) Characterization of the zero-bias photoelectric performance of the device in (c) under 0.04-THz irradiation. (e) The cross-sectional profile of $PdSe_2$ flake obtained by AFM scanning along the red dash line shown in (c). (f) Raman spectrum of the $PdSe_2$ flake.

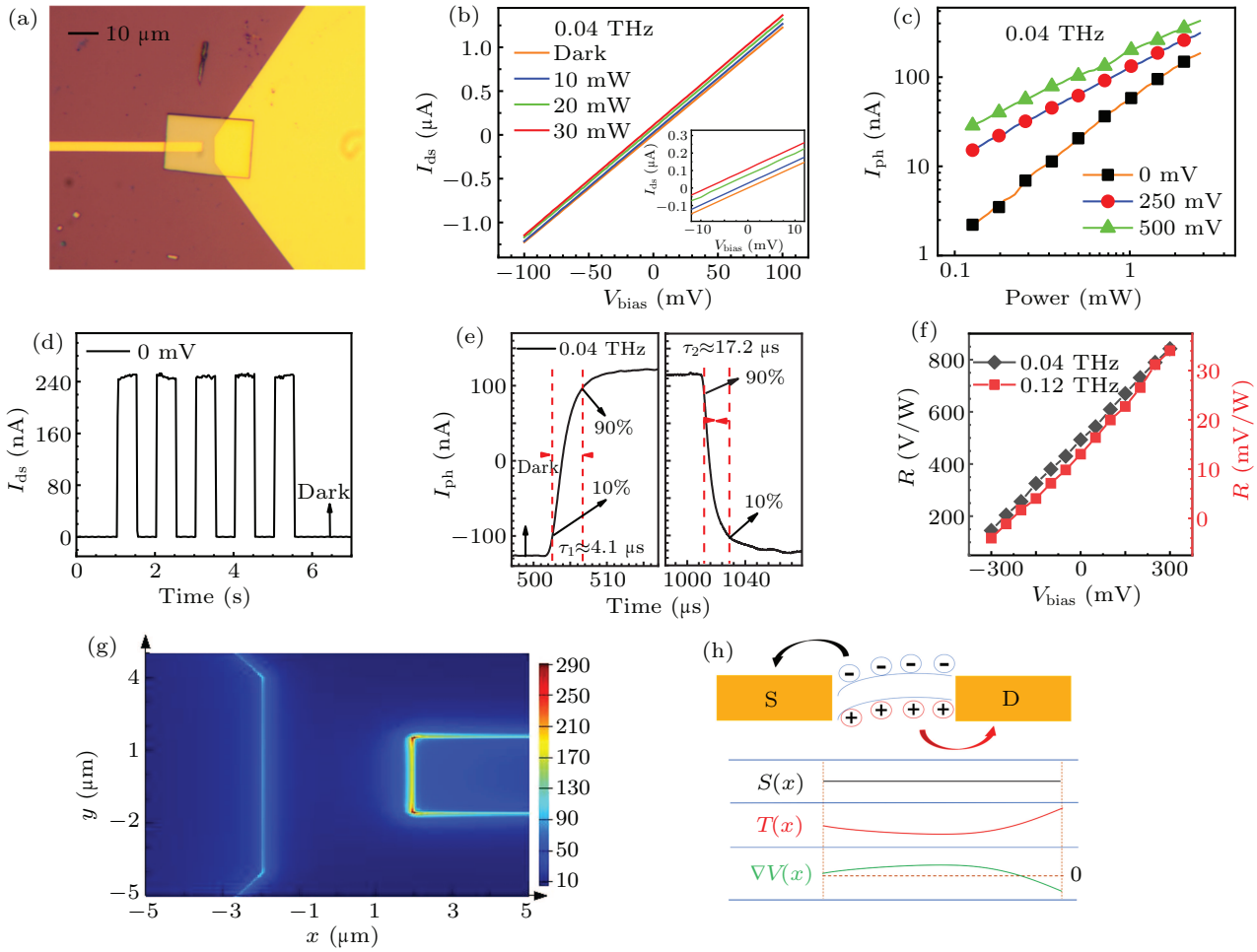


Fig. 2. Performance characterization of photodetector based on $PdSe_2$ with asymmetric eletron. (a) The optical imgae of the device with unilateral butterfly antenna. (b) Current–voltage (I–V) characteristics of the $PdSe_2$-based photodetector in the dark and under 0.04-THz irradiation with different incident powers. (c) I_{ph} as a function of incident power at different bias voltages. (d) Time-dependent photocurrents of the $PdSe_2$-based photodetector under switching on/off. (e) The rise and fall time of the photoresponse of the device. (f) The R_V of the device under 0.04-THz and 0.1-THz irradiations, respectively. (g) The electric field distribution of the device with unilateral butterfly antenna. (h) A schematic diagram of the PTE effect-dominated photoresponse.

To study the generation mechanism of photocurrent, we constructed a half-butterfly device as shown in Fig. 2(a). We evaluated the electrical properties of the device based on $PdSe_2$ in the dark. As shown in Fig. 2(b), I–V curves of the device show good Ohmic contact in a small current range from −5 mV to 5 mV. To study the optoelectronic properties of photodetector based on $PdSe_2$, the microwave source is used with a tunable power density to excite the photocurrent. The I–V curves as a function with bias voltage at different power densities were obtained under 0.04-THz irradiation as shown in Fig. 2(c), respectively, which exhibits a perfect linear relationship between I_{ph} and V_{bias}. In the small bias voltage range, it is obvious that the I_{ph}–V_{bias} curves shift upon light illumination, which is a typical feature of the PTE effect. In Fig. 2(b), I_{ph} is plotted as a function of power (P) with good linearity in double-logarithmic coordinates, which can also be expressed as a typical character of the PTE effect: $\log I_{ph} \propto \log P$.[20] The linear dynamic range (LDR) is an important performance of terahertz detector, defined as an optical power marginwithin which the output photocurrent is linearly proportional to optical signal input: $\mathrm{LDR} = 20 \times \log(P_{max}/P_{min})$. Due to the limitation of measurement equipment, we can calculate that the LDR of the photodetector is greater than 27 dB.

To explore the performance of the photodetector, the electromagnetic waves at 0.04 THz are modulated to illuminate the photodetector at RT under an ambient environment at a power density of 1.05 mW·cm^{-2}. Figure 2(d) shows the fast on/off switched photocurrents of the device at zero bias voltage, in which the pulse shape was well preserved. The response time is about 4.1 μs, and the decay time is about 17.2 μs, which is sufficient to meet the requirements of frame rate imaging.

The photocurrent generation mechanism can now be fully discussed based on the above results. It has been discovered that a variety of physical mechanisms may cause broadband response for the photodetector, including photoconductivity (PC) effect, photovoltaic (PV) effect, and pyroelectric effect (bolometric, PTE, and pyroelectric effect). The photon energy of microwave and THz is smaller than the energy bandgap of the $PdSe_2$. Therefore, the thermoelectric effect is related to the photo-induced hot carriers, but not to the the number of

particles and is independent of the incident wavelength. The photodetector responds without bias, which does not conform to the characteristics of the bolometric effect. As shown in Fig. 2(d), considering the device's time-dependent photocurrent characteristics obtained when switching the illumination on and off can exclude the pyroelectric effect. Therefore, the PC, PV, bolometric, and pyroelectric effects are eliminated, meaning that the PTE effect is responsible for the photoresponse of the device.

The critical parameters of photodetector performance were calculated from the measured photocurrent and plotted as a function of bias voltage in Fig. 2(f). R is defined as photocurrent response generated by per unit excitation light power on the effective area of the photodetector: $R = I_{\rm ph}/(P_{\rm in}S_\lambda)$, where $P_{\rm in}$ is the incident light power of the source that is irrelevant to the material and response mechanism, S_λ is the effective area of photodetector under long-wavelength irradiation. In this work, the effective area of the antenna is: $S_\lambda = \lambda^2/4\pi$, where λ is the wavelength of the radiation. As the bias voltage changes, the voltage responsivity of the device changes linearly. Then, to study the response of $PdSe_2$ at higher frequencies, the photocurrent response under 0.12-THz irradiation is also measured. Compared with the microwave range, the device's response under THz irradiation will drop by two orders of magnitude.

To further understand the PTE effect in our device, the driven mechanism of the photodetector is shown in Fig. 2(h). The PTE effect means that the entire device will form a temperature gradient under light illumination. Meanwhile, the generation of photocurrent relies on the transport of hot carriers.[21] Since the device's geometry and electric field distribution is not completely symmetrical, THz photoexcitation causes hot carriers to heat up unevenly and gives rise to the temperature gradients of electrons (in Fig. 2(g)). In the present work, an asymmetrical temperature within the $PdSe_2$ channel leads to a charge transfer among the contacts. The PTE effect is caused by the irregular shape of the exfoliated $PdSe_2$ flake and the disequilibrium electric field distribution of the device with a unilateral butterfly antenna. Definitely, the hot carriers create a potential gradient by the temperature difference: $\Delta V = S\Delta T$, where S is the Seebeck coefficient of $PdSe_2$ and ΔT is the temperature gradient of the device under light irradiation without bias voltage. In the bias mode, the photocurrent is affected by the PTE effect and modulated by the static electric field.

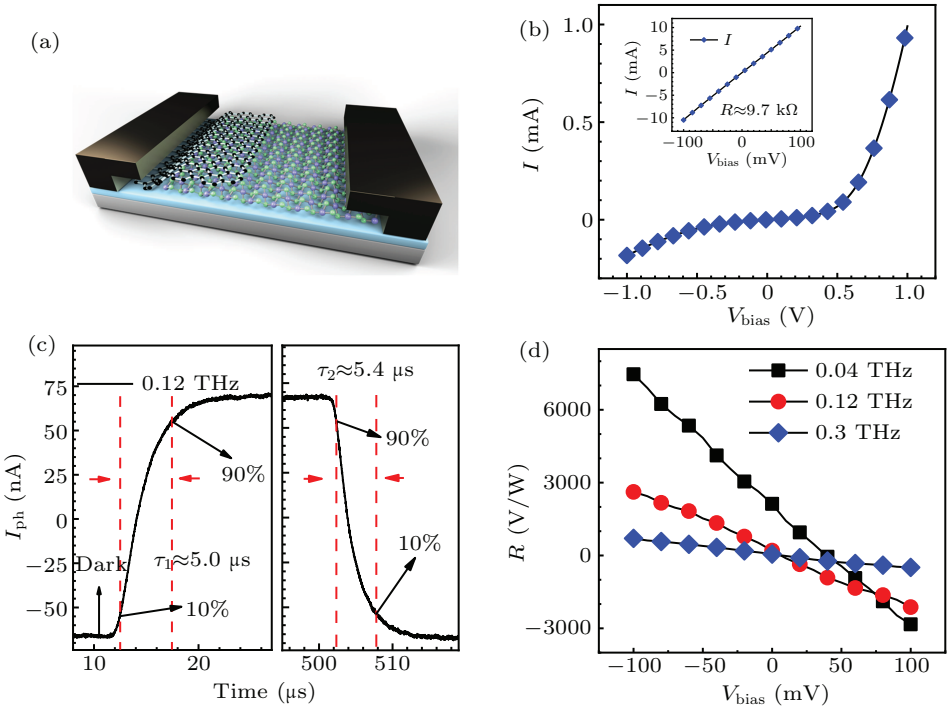


Fig. 3. (a) The 3D schematic diagram of the $PdSe_2$/graphene heterojunction photodetector with symmetric metal electrodes (Cr/Au). (b) The I–V characteristics of the $PdSe_2$/graphene heterojunction photodetector in the dark. (c) The response time of the $PdSe_2$/graphene heterojunction photodetector at 0.12 THz. (d) R of $PdSe_2$/graphene heterojunction photodetector under optical radiation of different frequencies.

Unlike bulk materials, the layers of two-dimensional materials are connected by weak van der Waals forces, which facilitate the formation of heterojunctions without causing other defects. If the THz photoexcitation heats the carriers and gives rise to a temperature gradient due to the asymmetry of device geometry, the PTE photocurrent can arise in the absence of bias accordingly. By forming p–n junction, interface junction, gate-control, asymmetric antenna, and asymmetric electrode materials, asymmetrical temperature distribution or Seebeck coefficient along the channel can be achieved.[22–26] Therefore, we want to engineer the S coefficient difference between graphene and $PdSe_2$ to enhance the PTE effect. A vdW hetero-

junction with a small lattice mismatch by stacking few-layer graphene with a $PdSe_2$ flake is shown in Fig. 3(a). Such vdW heterostructures can induce a larger built-in electric field than the traditional bulk semiconductor heterostructure due to the plentiful charge transfer among the layers. We still performed the above measuring procedure for the heterostructure device, and the *I*–*V* curve in Fig. 3(b) shows the typical characteristics of the PN junction in a large voltage sweep. The inset shows the *I*–*V* curve in the small bias voltage range shows good linearity and means that $PdSe_2$ and graphene form stable and good interface contact. Under the THz irradiation, the device exhibits a large *R* that maintains an excellent linear relationship with the bias voltage. Figure 3(c) shows the single on-off cycle to evaluate the response time of our detectors at 0.1 THz, respectively. The $PdSe_2$/graphene vdW heterojunction photodetector shows the rapid rise and fall times of 5.0 μs and 5.4 μs. With bias voltage, the device performance is also explored in Fig. 3(d).

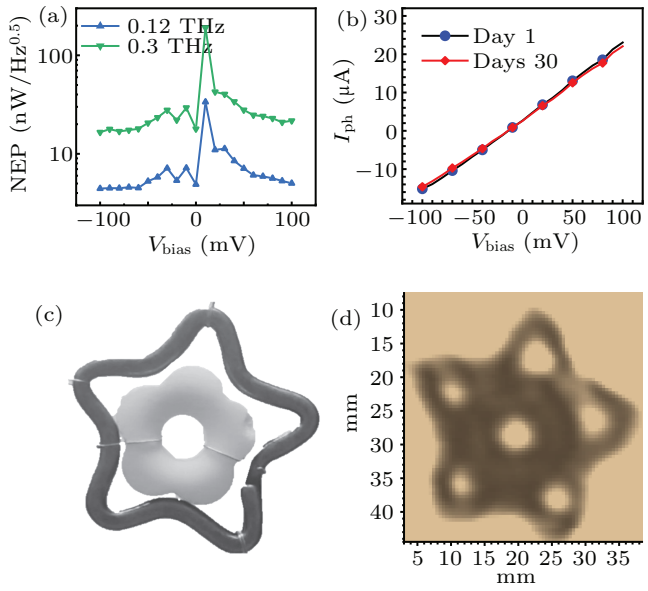


Fig. 4. Response mechanism of $PdSe_2$ photodetector with asymmetric metal electrodes and imaging of the $PdSe_2$/graphene heterojunction photodetector. (a) *R* and (b) NEP of $PdSe_2$/graphene heterojunction photodetector at optical radiation of different frequencies. (c) Stability of the $PdSe_2$/graphene heterojunction photodetector. The black spot represents the photocurrent of the as-fabricated device, while the red spot denotes the photocurrent of the device after 30 days in ambient atmosphere. (d) The imaging of the $PdSe_2$/graphene heterojunction photodetector at the zero-bias value of 0 mV at 0.3 THz.

From the perspective of practical applications, NEP is another crucial figure of merit to evaluate the performance of a photodetector, which is defined as the lowest detectable power in 1-Hz bandwidth, and can be expressed as NEP = v_n/R_v, and v_n is the root mean square of the noise voltage and R_v is the voltage responsivity of the device. The bias-voltage dependence of noise equivalent power (NEP) is shown in Fig. 4(a).[27] Remarkably, when a bias voltage is applied across the device, the value of the noise will not change significantly. Through experiments, we found that, differently from black phosphorus, photodetector based on $PdSe_2$ exhibits better stability.[28] We measured the photocurrent of the heterostructure device under 0.1-THz radiation and compared the change of the photocurrent before and after the exposure for one month. As shown in Fig. 4(b), the photocurrent of the device is repeatable without apparent degradation, indicating the excellent stability of our device. The high-contrast THz imaging is obtained at zero bias clearly shows the shape of the concealed object. We can see that the outline of THz imaging for the five-pointed star metal-buckle and the circular sugar pill shown in Fig. 4(d) is consistent with the optical picture in Fig. 4(c). Hence, the self-powered, high Sensitivity, and stability of the THz photodetector based on $PdSe_2$, show good advantages for future THz detection applications.

4. Conclusion and perspectives

To summarize, we have designed and fabricated THz photodetector based on $PdSe_2$ with asymmetrical electrode structure, enabling self-powered detection capability at room temperature. The device generates a large photocurrent under zero bias, indicating that the primary photoresponse of the device comes from the PTE effect. In addition, we found the stronger photovoltage and higher performance generated by the PTE effect through introducing the $PdSe_2$/graphene vdW heterostructure. Furthermore, $PdSe_2$ with a corrugated pentagonal structure guarantees excellent device stability even when exposed to the air for a sustained period. Considering the high Sensitivity, broadband detection capability, and remarkable stability, the $PdSe_2$/graphene heterostructure photodetector demonstrates the imaging ability at 0.3 THz. We have confirmed the potential of the $PdSe_2$ for practical applications in the terahertz range for the first time.

Acknowledgements

Project supported by the National Natural Science Foundation of China (Grant Nos. 61521005, 61875217, 91850208, 61474130, and 62075230), the Natural Science Foundation of Shanghai, China (Grant Nos. 19ZR1465400, 21ZR1473800, and 20142200600), and the Fund from Zhejiang Laboratory (Grant No. 2021MB0AB01).

References

[1] Siegel P H 2002 *IEEE Trans. Microw Theory Tech.* **50** 910
[2] Horiuchi N 2010 *Nat. Photon.* **4** 140
[3] Tonouchi M 2007 *Nat. Photon.* **1** 97
[4] Nagatsuma T 2011 *IEICE Electron. Expr.* **8** 1127
[5] Ajakaiye O, Grade J, Shin C and Kenny T 2007 *Sens. Actuator A Phys.* **134** 575
[6] Miao W, Gao H, Wang Z, Zhang W, Ren Y, Zhou K M, Shi S C, Yu C, He Z Z, Liu Q B and Feng Z H 2018 *J. Low Temp. Phys.* **193** 387
[7] Vining C B 2009 *Nat. Mater.* **8** 83
[8] Boukai1 A I, Bunimovich Y, Tahir-Kheli J, Yu J K, Goddard III W A and Heath J R 2008 *Nature* **451** 168

[9] Sun J F, Shi H L, Siegrist T and Singh D J 2015 *Appl. Phys. Lett.* **107** 153902

[10] Lan Y S, Chen X R, Hu C E, Cheng Y and Chen Q F 2019 *J. Mater. Chem. A* **7** 11134

[11] Wang C and Gao G Y 2020 *J. Phys. Condens. Matter* **32** 205503

[12] Guo C, Guo W L, Xu H, Zhang L B, Chen G, D'olimpio G, Kuo C N, Lue C S, Wang L, Politano A, Chen X S and Lu W 2020 *2D Mater.* **7** 035026

[13] Novoselov K S, Mishchenko A, Carvalho A and Castro Neto A H 2016 *Science* **353** aac9439

[14] Liang Q J, Wang Q X, Zhang Q, Wei J X, Lim S X D, Zhu R, Hu J X, Wei W, Lee C K, Sow C H, Zhang W J and Wee A T S 2019 *Adv. Mater.* **31** 1807609

[15] Wu D, Guo J W, Du J, Xia C X, Zeng L H, Tian Y Z, Shi Z F, Tian Y T, Li X J, Tsang Y H and Jie J S 2019 *ACS Nano* **13** 9907

[16] Kang X L, Lan C Y, Li F Z, Wang W, . Yip S P, Meng Y, Wang F, Lai Z X, Liu C T and Ho J C 2021 *Adv. Opt. Mater.* **9** 2001991

[17] Mak C H, Lin S H, Rogee L and Lau S P 2020 *J. Phys. D: Appl. Phys.* **53** 065102

[18] Afzal A M, Iqbal M Z, Dastgeer G, Ahmad A U and Park B 2021 *Adv. Sci.* **8** 2003713

[19] Zeng L H, Wu D, Lin S H, Xie C, Yuan H Y, Lu W, Lau S P, Chai Y, Luo L B, Li Z J and Tsang Y H 2019 *Adv. Funct. Mater.* **29** 1806878

[20] Castilla S, Terres B, Autore M, Viti L, Li J, Nikitin A Y, Vangelidis I, Watanabe K, Taniguchi T, Lidorikis E, Vitiello M S, Hillenbrand R, Tielrooij K J and Koppen F. H L 2019 *Nano Lett.* **19** 2765

[21] He X W, Wang X, Nanot S, Cong K K, Jiang Q J, Kane A A, Goldsmith J E M, Hauge R H, Leonard F and Kono J 2013 *ACS Nano* **7** 7271

[22] Xu X D, Gabor N M, Alden J S, van der Zande A and McEuen P L 2010 *Nano Lett.* **10** 562

[23] Echtermeyer T J, Nene P S, Trushin M, Gorbachev R V, Eiden A L, Milana S, Sun Z, Schliemann J, Lidorikis E, Novoselov K S and Ferrari A C 2014 *Nano Lett.* **14** 3733

[24] Viti L, Hu J, Coquillat D, Knap W, Tredicucci A, Politano A and Vitiello M S 2015 *Adv. Mater.* **27** 5567

[25] Leong E, Suess R J, Sushkov A B, Drew H D, Murphy T E and Mittendorff M 2017 *Opt. Express* **25** 12666

[26] Zuev Y M, Chang W and Kim P 2009 *Phys. Rev. Lett.* **102** 096807

[27] Liu C L, Wang L, Chen X S, Zhou J, Hu W D, Wang X R, Li J H, Huang Z M, Zhou W, Tang W W, Xu G Y, Wang S W and Lu W 2018 *Carbon* **130** 233

[28] Guo W L, Dong Z, Xu Y J, Liu C L, Wei D C, Zhang L B, Shi X Y, Guo C H, Xu H, Chen G, Wang L, Zhang K, Chen X S and Lu W 2020 *Adv. Sci.* **7** 1902699